Biochimica et Biophysica Acta 1847 (2015) 86–97

Contents lists available at ScienceDirect

Biochimica et Biophysica Acta

journal homepage: www.elsevier.com/locate/bbabio

Review

Infrared and Raman spectroscopic investigation of the reaction mechanism of cytochrome *c* oxidase ☆

Satoru Nakashima [a], Takashi Ogura [a,b], Teizo Kitagawa [a,*]

[a] Picobiology Institute, Graduate School of Life Science, University of Hyogo, RSC-UH Leading Program Center, 1-1-1 Koto, Sayo-cho, Sayo-gun, Hyogo 679-5148, Japan
[b] Department of Life Science, Graduate School of Life Science, University of Hyogo, RSC-UH Leading Program Center, 1-1-1 Koto, Sayo-cho, Sayo-gun, Hyogo 679-5148, Japan

ARTICLE INFO

Article history:
Received 28 April 2014
Received in revised form 7 July 2014
Accepted 11 August 2014
Available online 16 August 2014

Keywords:
Cytochrome *c* oxidase
Proton-pumping mechanism
Time-resolved infrared and
Raman spectroscopy

ABSTRACT

Recent progress in studies on the proton-pumping and O_2 reduction mechanisms of cytochrome *c* oxidase (CcO) elucidated by infrared (IR) and resonance Raman (rR) spectroscopy, is reviewed. CcO is the terminal enzyme of the respiratory chain and its O_2 reduction reaction is coupled with H^+ pumping activity across the inner mitochondrial membrane. The former is catalyzed by heme a_3 and its mechanism has been determined using a rR technique, while the latter used the protein moiety and has been investigated with an IR technique. The number of H^+ relative to e^- transferred in the reaction is 1:1, and their coupling is presumably performed by heme *a* and nearby residues. To perform this function, different parts of the protein need to cooperate with each other spontaneously and sequentially. It is the purpose of this article to describe the structural details on the coupling on the basis of the vibrational spectra of certain specified residues and chromophores involved in the reaction. Recent developments in time-resolved IR and Raman technology concomitant with protein manipulation methods have yielded profound insights into such structural changes. In particular, the new IR techniques that yielded the breakthrough are reviewed and assessed in detail. This article is part of a Special Issue entitled: Vibrational spectroscopies and bioenergetic systems.

1. Introduction

CcO is the terminal enzyme of the respiratory chain and catalyzes O_2 reduction coupled with protons being pumping across the inner mitochondrial membrane. CcO consists of four redox-active metal centers, Cu_A, heme *a*, heme a_3 and Cu_B [1]. The electrons given to Cu_A by cytochrome *c* are transferred to the heme a_3–Cu_B binuclear center (BNC) through heme *a*. In order to reduce an O_2 molecule trapped at heme a_3 to H_2O, a single electron transfer from Cu_A to the BNC is repeated for four times, and the BNC changes through several intermediate states denoted by E, R, A, P, F and O as illustrated in Fig. 1 [2]. The electronic structure and behavior have been studied extensively with the rR technique [2], and are essentially the same for bovine and bacterial CcOs. In contrast, there are distinct differences between the two kinds of enzymes regarding the H^+ pathway. For bacteria, the protons used to generate H_2O molecules (chemical H^+) and the protons that are pumped are both transferred from the negative side of the membrane to the O_2 reduction site through the K- and D-pathways and there is no other pathway [1]. For bovine heart CcO, however, H^+ is pumped through another network known as the H-pathway, while chemical H^+ passes through the K- and D-pathways [3–6].

The crystal structures of many protonmotive CcOs have been established [4,7–11]. For example, recent progress in structural studies of bovine heart CcO has revealed not only the resting state, but also the structures of models of transient species by using various O_2 analog molecules [9]. It has thus become clear that the binding of a strong ligand to heme a_3 induces a conformation change that significantly narrows the water channel and effectively blocks the back-leakage of protons from the hydrogen bond network, as discussed below. Fig. 2 shows one portion of the bovine CcO structure that is related to the reaction site and water channel.

The similarities and differences in the roles of a few key residues between bovine and bacterial CcOs have been discussed [2,3,12–17]. The 1:1 coupling in H^+/e^- transfers appears to be essential for the functioning of CcO. The chemical and physical factors that govern the coupling are the key points that remain to be solved, and the analysis requires temporal as well as static traces of the reaction under physiological conditions. Although IR spectroscopy is known as a powerful technique for meeting such requirements, there has been a serious problem with applying it to CcO, because solvent H_2O potently absorbs IR light, so the faint signals from the protein are obscured.

Abbreviations: CcO, cytochrome *c* oxidase; IR, infrared; rR, resonance Raman; TR, time-resolved; BNC, binuclear center; ATR, attenuated total reflectance; FT, Fourier transform; MV, mix valence; FR, fully reduced; DFG, difference frequency generator; OPA, optical parametric amplifier; COV, CcO contained in phospholipids vesicles; TR^3, time-resolved resonance Raman; CW, continuous wave; Mb, myoglobin

☆ This article is part of a Special Issue entitled: Vibrational spectroscopies and bioenergetic systems.

* Corresponding author. Tel./fax: +81 791 58 1967.
E-mail address: teizo@sci.u-hyogo.ac.jp (T. Kitagawa).

http://dx.doi.org/10.1016/j.bbabio.2014.08.002
0005-2728/

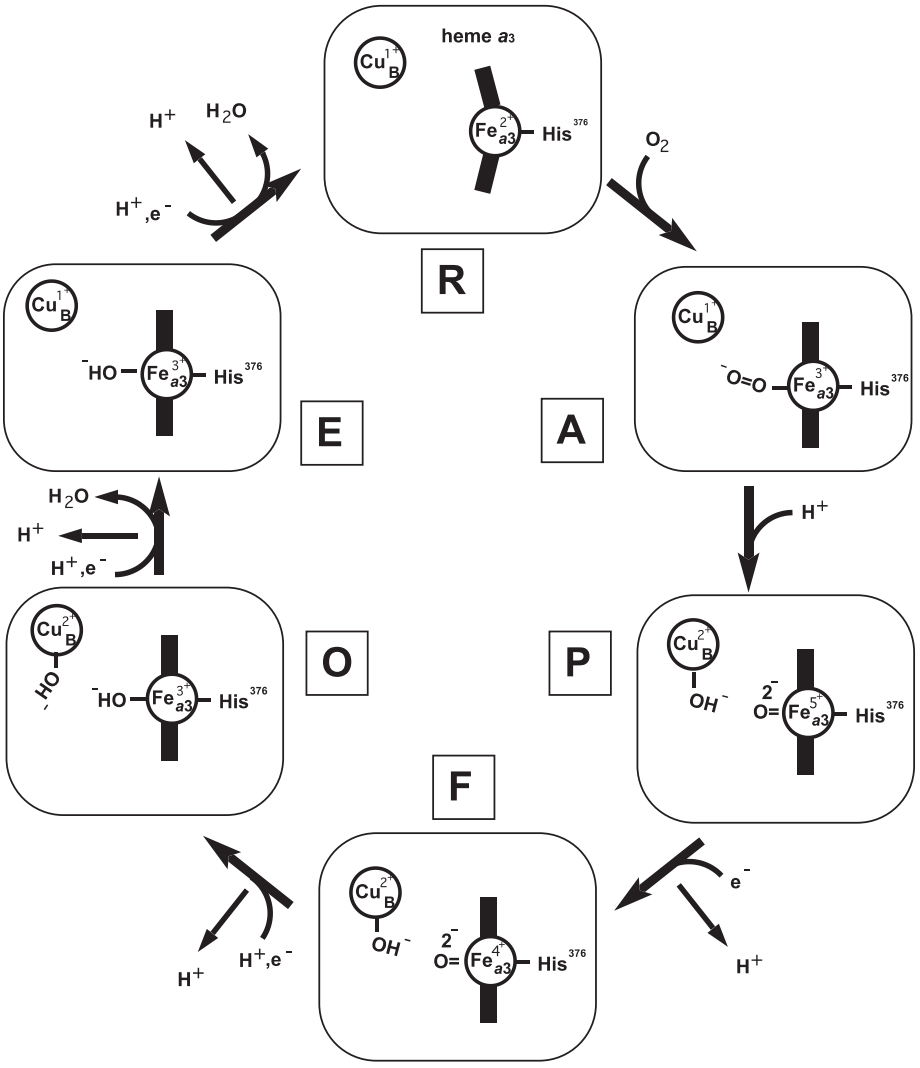

Fig. 1. Catalytic cycle of cytochrome *c* oxidase (CcO). The rectangle represents the BNC, which includes heme a_3 and Cu_B.

In this article, the considerable efforts performed under these arduous conditions (Subsection 2.1) and certain ingenious methods developed recently to overcome them [2,20–22] will be reviewed first (Subsection 2.2). The new technique [18,19], which made a breakthrough in the observation of a structural change of a single residue from ~1800 residues of bovine CcO upon CO photo-dissociation, will be explained in detail (Subsection 2.3) and the results obtained from it thus far will be assessed (Section 4), accompanied by the rR results (Section 3).

2. Infrared spectroscopic studies

IR spectroscopy is a method for probing structural changes of functional groups at a level of a single chemical bond and can provide clear information on the protonation of a particular residue. Carboxylic acid side chains in heme as well as glutamic and aspartic acid may play a key role in intra-protein H^+ transfers by direct protonation or by rotation around the C – COOH bond [23,24], and such changes have been detected in the mid-IR range [25–28]. The amide I band reflects the main-chain structure of a protein and the empirical relationships between the band positions and secondary structures, such as α-helix, β-sheet and random coil, have been established [27]. It was reported that a partially disordered α-helix gives an amide-I band at a higher-than-usual wavenumber [29,30]. Protonatable side chains such as Tyr also yield information about the intermediate state [31–33]. Furthermore, the ordered H_2O molecules that form an extended hydrogen bond network which may play an essential role in H^+ transfer were discussed with IR spectra [34–36]. Although IR spectroscopy has a potential to provide such important structural information, it has fundamental restrictions to hinder the observation in natural conditions. Many ingenious methods have been devised to overcome the restrictions and indeed gave fruitful results. In this section, the restrictions that make IR measurements difficult are briefly surveyed, and the efforts to overcome them are reviewed.

2.1. Difficulties in utilizing IR spectroscopy for CcO

First, H_2O exhibits potent IR absorption at ~1650 cm^{-1} (bending mode) and ~3400 cm^{-1} (symmetric stretching mode). The former band hides the various important protein bands mentioned above. Concentrated protein solution in the form of a thin film (<10 μm) may be used outside of the two bands. An attenuated total reflection (ATR) method was applied successfully to stable intermediates of hydrated CcO [37].

Second, the restriction arises from the principle of the Fourier-Transform (FT) IR technique itself [38], although its advantage compared

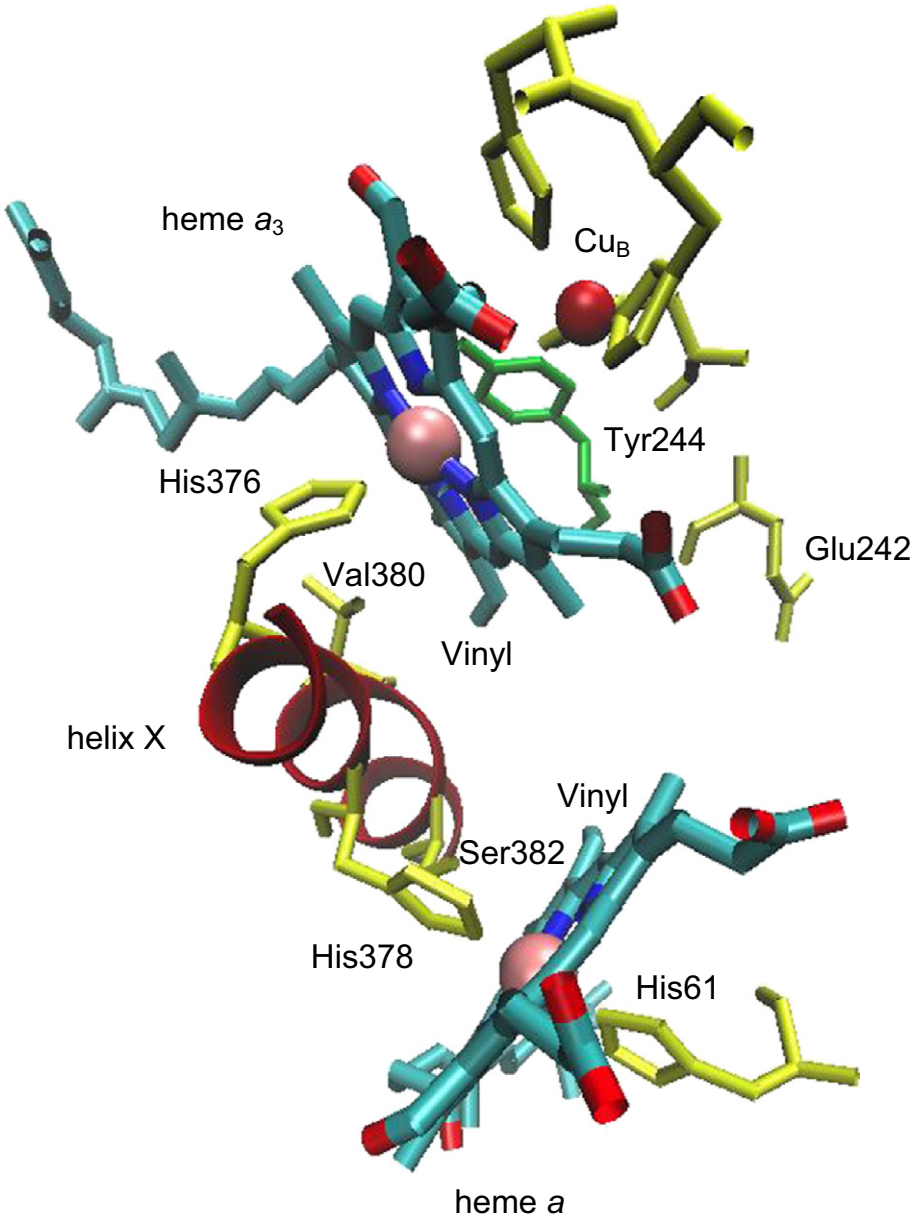

Fig. 2. A part of the bovine CcO structure, which relates to the oxygen reduction reaction site and water channel. The figure shows BNC (heme a_3, Cu_B), heme a, their ligands (His376, His378, and His61) and certain critical amino acids in the D- (Glu242), K- (Tyr244) and H-pathways (Val380 and Ser382). Structural data were taken from PDB (2EIJ) and the figure was prepared with VMD (Visual Molecular Dynamics) program.

with the traditional dispersion type is well recognized and indeed, commercial FTIR spectrophotometers have been developed that yield excellent signal/noise (S/N) ratios and stability. Since the FT method utilizes a broad band of radiation and all of the bands interfere with each other, this becomes a serious problem when absorbance of a certain band exceeds the upper limit. The averaging procedures used are able to determine the correct spectrum for a weak band buried in a huge background absorption that is even 10^5 times greater. Practically, however, the absorbance of the sample must be less than ~1 O.D. in the whole range of the band. This means that the thickness of the cell must be <10 μm for H_2O solutions when the spectral range includes ~1650 cm^{-1} regions, and consequently the protein concentration must be very high to successfully obtain any signals from the proteins. Another defect of FTIR is the inability to accumulate spectra for a longer time for a particular band in question, because it is based on single-point detection and therefore the spectra in the whole range must be accumulated for the same period. This takes a long time and there is no capacity for improving the S/N ratios for a selected band.

The third point to be noted for IR spectroscopy is that all of the residues have nearly equal absorption rate and it is exceedingly difficult to assign an observed spectral change to a particular residue. An observed spectral change is typically infinitesimal compared with the 10^5 times greater background absorption. So it is desirable to detect only the localized changes that have been induced in some way. In other words, it would be preferable to record a difference in the spectra between two defined states in which the huge unchanged background was canceled out. To improve the spectral quality, it is required that the two defined states are generated in a cyclic and repetitive manner without perturbing other parts of the protein. Even with such difference spectra, the IR bands of the

different residues are severely overlapped, so global fitting of the bands among the correlated spectra is required for analysis.

2.2. Ingenious method in IR studies

To overcome the difficulties mentioned above, various ingenious techniques have been applied to CcO and they are reviewed here. The most commonly used method is the utilization of photochemical reactions. Photolysis of heme a_3–CO has been applied to transmission difference IR spectra [39–60]. A spectroelectrochemical IR cell that inserts an optically transparent thin layer electrode was used to change redox states of metal centers [20,21,31,61–66]. ATR is an alternative method for measuring the reaction [22,32,33,59,67–72], in combination with mutagenesis in the bacterial CcO case.

In the initial IR studies of CcO, CO was used as a marker ligand that can control the reaction and dynamics of the proteins [39–42] and also for comparison among the different electronic states, such as fully-reduced (FR), mixed-valence (MV) and other intermediate states [50–52,56–60]. In the time-resolved measurements using CO-photolysis, the time range spread was from pico- [43–45] to millisecond [44,53–55]. It became clear from those observations that CO photo-dissociated from heme a_3^{2+} binds to Cu_B that is located just above heme a_3 in ~1 ps, and escapes into the bulk solution in ~2 μs. The rebinding of extraneous CO to heme a_3^{2+} occurs within a few tens of ms. The time scales for these events are quite different and seem to reflect the dynamical properties of the corresponding parts of the protein.

On the other hand, precise IR difference spectra were obtained by using photo-steady states composed of stable intermediates. For example, the differences in the bands between the presence and absence of photodissociating pump light for the CO-adducts, which were detected at 1737 and 1749 cm^{-1}, were assigned to the protonation of key carboxylic acid residues, Asp51 and Glu242, respectively, of bovine CcO [56] (bovine sequence numbering is used throughout, unless indicated otherwise). By the use of an electrochemical IR cell, the difference between the reduced and oxidized forms of whole CcO was investigated; the peaks at 1746 and 1734 cm^{-1} were assigned to the oxidized and reduced forms, respectively [61,62]. In the case of bovine heart CcO, 1738 cm^{-1} and 1585 cm^{-1} bands are assignable to COOH and COO^- of Asp51, respectively [4,56,62]. Since there is no redox-coupled conformational change in the carboxyl groups except for Asp51 is evident in the X-ray structures, it is assumed that Asp51 is the exit of the proton in the H-pathway, at least in bovine heart CcO. The infrared spectral changes were due to a single electron equivalent, and heme *a* was able to be assigned as the metal site controlling the conformation of Asp51 [4]. The carboxyl modes of heme *a* and heme a_3 were also assigned and it was clarified that the ring-D propionate of heme *a* is the likely H^+ acceptor upon the reduction of CcO, and that the ring-D propionate of heme a_3 either undergoes conformational changes or, less likely, acts as a H^+ donor [63,64].

With the ATR method [22], the internally reflected IR beam at the surface of a prism penetrates into the sample attached to the prism as an evanescent wave. The penetration depth in the mid-IR range is a few microns. Thus, the IR spectra of protein films on the prism surface can be observed without the disturbance by H_2O bands. This technique allows easy access to the sample on the prism and particularly enables a perfusion of reagents over the protein surface. By using this technique [64–71], the carboxyl bands observed for the P_M and F intermediates were assigned, and Glu242 was confirmed to be deprotonated in P_M and O, and reprotonated in F, suggesting a role for Glu242 as a H^+ shuttle in the D-pathway.

Low temperature measurements helped to clarify the IR spectra. The IR spectra of CcO at −20 °C exhibited a band at 1745 cm^{-1} in H_2O and this was assigned to Glu242 at the end of the D-pathway [54]. Mutants that have inhibited reactions [59,60,68,69] were used for real-time measurements of bacterial CcO by ATR-FTIR spectroscopy; for instance, a reaction with O_2 was investigated with a D124N mutant (*Paracoccus denitrificans* number) having a blocked D-pathway of H^+ transfer [68]. These observations confirmed that the protons required for the chemistry at the BNC are taken from Glu242 in the P to F step.

The information obtained from these experiments is helpful, but there are questions that remain due to the non-physiological conditions of the experiments. It is known that CO binds to Cu_B instead of heme a_3 at low temperatures. This means that the protein structure and/or potential energy minima must be altered by temperature, and the reaction mechanism is thereby affected. Mutation of a residue important for the reaction may influence the H^+ transfer pathway. Therefore, the development of new IR technology is needed to obtain information on the physiological processes that are operative at room temperature.

2.3. Newly developed IR spectroscopy

2.3.1. The advantages of the new method

A novel nanosecond TRIR spectrometer that has demonstrated excellent performance in investigating the reactions of CcO in H_2O solution was developed by Nakashima [19] and Kubo [18]. Since this system is able to overcome many of the problems mentioned in Subsection 2.1, this section details certain fundamental features of the new technique. Fig. 3 depicts the schematic diagram of the apparatus.

A femtosecond IR laser is employed as the IR light source. Concretely, a femtosecond mid-IR pulse (>10 μJ/pulse, ~50 fs) with a spectral width of 350 cm^{-1} was produced by a difference frequency generator (DFG) with an optical parametric amplifier (OPA), which was pumped by the output of an integrated Ti:sapphire oscillator/regenerative amplifier system operating at 1 kHz. The advantage of the brightness (a peak power of 0.2 GW in the mid-IR region) of the femtosecond pulse is in order to detect a substantial number of photons after transmission through H_2O. Since the pulse duration of the laser is on the order of a femtosecond, the interaction of IR light with the sample takes place on a very short time scale. Thus, the effect of photo-damaging the sample can be safely ignored during observations conducted using this pulse.

The second benefit of employing a femtosecond laser is its broad bandwidth. An IR spectrum of 350 cm^{-1} width can be measured in a single shot using a detector array of MCT elements coupled to a spectrograph. Compared with FTIR, in which a scanning interferometer is necessary, this reduces the accumulation time drastically. When the detector is a dual-row array, the signals generated by the probe and reference pulses are detected with the upper and lower arrays independently and simultaneously. For each laser shot, the spectrum of a sample is obtained from the intensity ratios of the two simultaneously observed spectra. This compensates for the laser pulse fluctuation. The dispersive configuration of the spectrometer is effective in focusing on only a selected wavenumber region; for CcO in H_2O, the measurements were focused on the 1750–1500 cm^{-1} range with strong absorbance, but eliminated in the weak absorption region (e.g., 1800–2100 cm^{-1}). This enables the use of a high power light without saturation of a detector. Furthermore, the use of a multi-channel detector enables signal amplification with an adjustable gain for each channel independently. The selection of the wavenumber regions and gain adjustment for each wavenumber cannot be performed with FTIR, because a single channel detector must be used and the amplifier gain is common to all of them. This is important in order to achieve a high sensitivity for the amide I band of CcO in H_2O solution. As a result, the resolution of the system is ~2 cm^{-1}, which is comparable with ordinary FTIR and adequate for identifying general protein bands.

The third characteristic of the system is associated with the improvement of the spectral quality by a measurement algorithm. The second laser, an Nd:YAG laser 25-ns with 532-nm output (0.15 mJ) at 1 kHz was used as a pump pulse for initiating the photodissociation reaction. It is noted that the pulse duration of this laser determines the whole time-resolution of the system. The pump beam was modulated using a phase-locked chopper operating at 0.5 kHz, which allowed nearly simultaneous (1 ms interval) measurements of the pump-on and

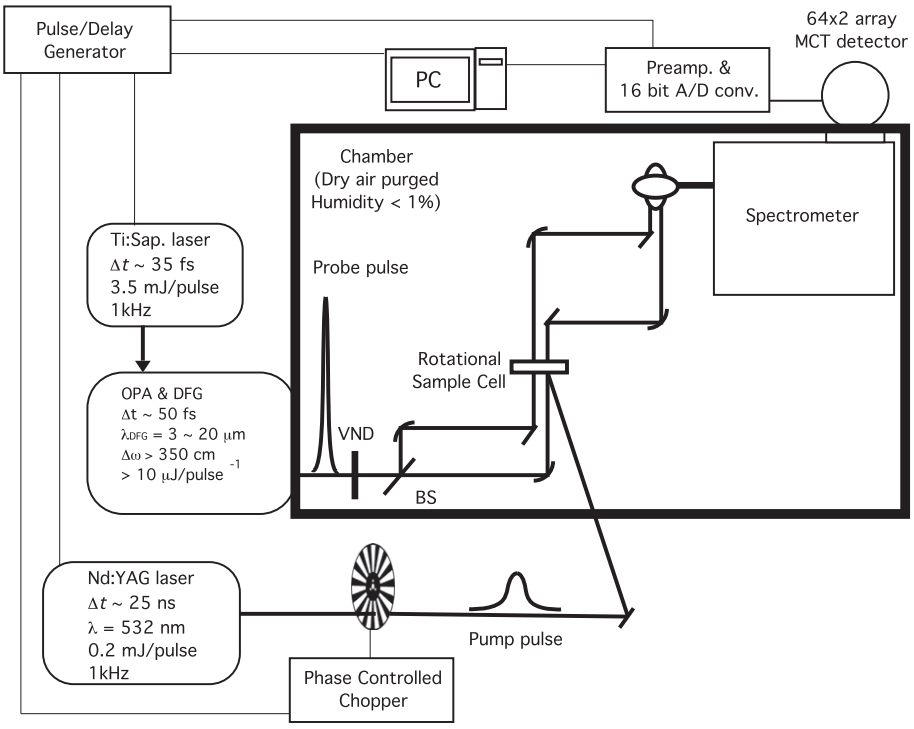

Fig. 3. Schematic diagram of the newly developed TRIR spectrometer. See the text for the detail of each component. Abbreviations: VND, variable neutral density filter; BS, beam splitter.

pump-off spectra. The present algorithm records the difference between these pump-on and pump-off spectra. As was mentioned in Subsection 2.1, it is important in the case of IR spectra to obtain the difference between two defined states. Another characteristic emerged from data analysis, in which statistical and mathematical methods were applied. Artificial noise, such as that arising from the power supply (60 Hz, west Japan) was removed completely.

As a result of these combined efforts, spectra with high S/N ratios were obtained in a relatively rapid accumulation time. Usually a laser pulse has a 2% peak-to-peak fluctuation, but the dual array detection compensated for this fluctuation and raised the S/N ratio 10 times. The algorithm and analysis of the data ensure that the fluctuation of the data is absolutely stochastic, and this n times accumulation of the data surely increases the S/N ratio by $n^{1/2}$ times. As the laser is operated at 1 kHz, 10 second accumulation corresponds to 10,000 accumulations of spectra, which increases the S/N ratio by nearly 100 times. On the whole, a 2% fluctuation of laser shots was reduced to ~0.002% which corresponds to an ~10 μO.D. absorbance difference, in only 10 s of accumulation, even for H_2O.

The reduction in the data acquisition time brought about resulted in certain unique features in the analysis. Since many transient spectra were obtainable with the same sample, precise band shape analysis for the temporal profile of the spectra was achieved. The obtained TRIR difference spectra were analyzed in terms of global fit, where each band was supposed to have a Gaussian shape, and the time dependence of its amplitude was fitted by a single exponential rise or decay. Prior to setting the Gaussian bands, a singular value decomposition analysis was applied to extract the major principal components of the spectral changes. These procedures enable detailed band shape analysis even in regions in which various bands overlap with each other.

2.3.2. The performances of the new system

The TRIR system described above yields nanosecond TR spectra with a sensitivity of 30 μO.D. on the background of 2 O.D. for the amide I region of CcO in H_2O in only a 1 minute accumulation period. Fig. 4 provides an example that shows the sensitivity of the system around the amide I band region where the strong H_2O band is overlapped. The standard deviations in the figure come from the measurements of differently prepared batches of CcO on different days. This result clearly shows that the total S/N ratio of the system, including the different samples and conditions, is on almost the same order as that calculated theoretically (Subsection 2.3.1). Thus the performance of the system can be regarded as reaching approximately the limit of the measurability.

Another significant advantage of this system is that the spectral quality on the nanosecond time scale is as high as the μs time scale. This is due to the fact that the data acquisition of the TR spectra with signal amplification and digitization on a nanosecond time resolution

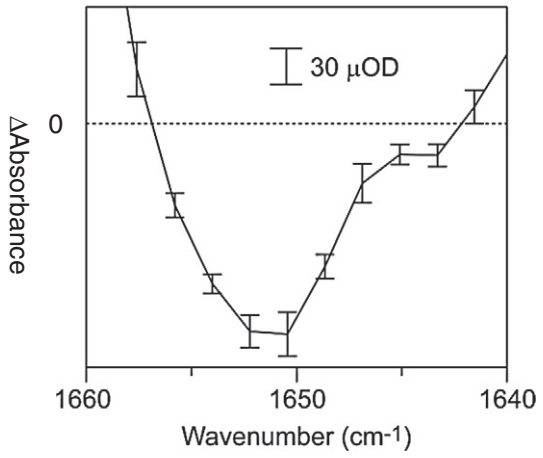

Fig. 4. Experimental accuracy in a spectral region against a strong background absorption (OD of 2). The TRIR difference spectrum of CcO at 50 μs after CO photolysis is depicted. The error bars represent the standard deviation of five independent experiments (each performed with 48 s of data accumulation) on different days using differently prepared batches of CcO. (Reproduced from Ref. [18].)

is not limited by the response speed of the detector electronics, in contrast to the step-scan FTIR system. The highest performance in the nanosecond step-scan FTIR system reported thus far is a sensitivity of 100 μO.D. on a background of 1 O.D. in a data accumulation time period of 2 h [73]. The data accumulation time and allowable background absorbance are both critical for a practical application of the system to H_2O solutions of CcO. Although extensive efforts have been made to obtain TRIR spectra with a short laser pulse [74–77], to the best of the authors' knowledge, there is no other IR system that is applicable to the investigation of CcO in H_2O with the present sensitivity and time-resolution at an ambient temperature.

2.3.3. The results obtained from the new TRIR system

Here, the results obtained from application of the new system to CcO in H_2O [18,19] are concretely described. They are associated with the nano- to micro-second dynamics of FR CcO upon CO photodissociation at ambient temperature, and it is presumed that the reverse process would correspond to ligand binding. In practice, spectra from 1500 to 2100 cm^{-1} were observed in a time range from 50 ns to 100 μs.

Fig. 5 shows the TRIR difference spectra, (pump-on)–(pump-off), of CcO in H_2O buffer. The positive and negative peaks appear from the photodissociated product and the non-photodissociated molecules, respectively. Accordingly, the negative peak at 1965 cm^{-1} arises from Fe-bound C–O stretching and the positive peak at 2063 cm^{-1} arises from Cu-bound C–O stretching (Fig. 5A). The peak intensity of the negative peak remains unaltered between 50 ns and 50 μs after CO-photolysis, indicating no geminate recombination of photodissociated CO (Fig. 5B). In contrast, the intensity of the positive peak decreases rapidly, indicating that photodissociated CO binds to Cu_B in a short time, but is released into the to solvent with a time constant of ~1.6 μs. This pattern of CO dynamics is consistent with previously reported results [41–44] and it should be emphasized that CO does not rebind to heme a_3 at all, even though it is more stable and hence better able to bind to heme a_3 in the stationary state.

The same types of difference spectra in the amide I region are illustrated in Fig. 5C, where 12 different bands were distinguished and their temporal behaviors analyzed separately. The most prominent feature is the peak/trough at 1666 cm^{-1}/1655 cm^{-1}. These two bands appeared just after the photodissociation (<50 ns) and decay with a time constant of 2.2 μs and 1.8 μs, respectively. Since the S/N ratios of the spectra are sufficiently high, analysis of the data allowed a determination of the precise band positions and shapes, so it became possible to estimate the intensity of these bands quantitatively. The molar absorption coefficient of the peak/trough is calculated to be 995 M^{-1} cm^{-1}, whereas the molar absorption coefficient of amide-I is reported to range from 200 to 1000 M^{-1} cm^{-1}, depending on the structures and microenvironments of the peptide C═O. Therefore, 1–5 C═O groups are involved in the transition from 1666 to 1655 cm^{-1}.

It has been reported that a partially disordered α-helix with a bulge structure provides an amide-I band at a higher-than-usual frequency (>1660 cm^{-1}) [29,30]. This is consistent with the general understanding that engagement of the peptide C═O with a hydrogen bond causes

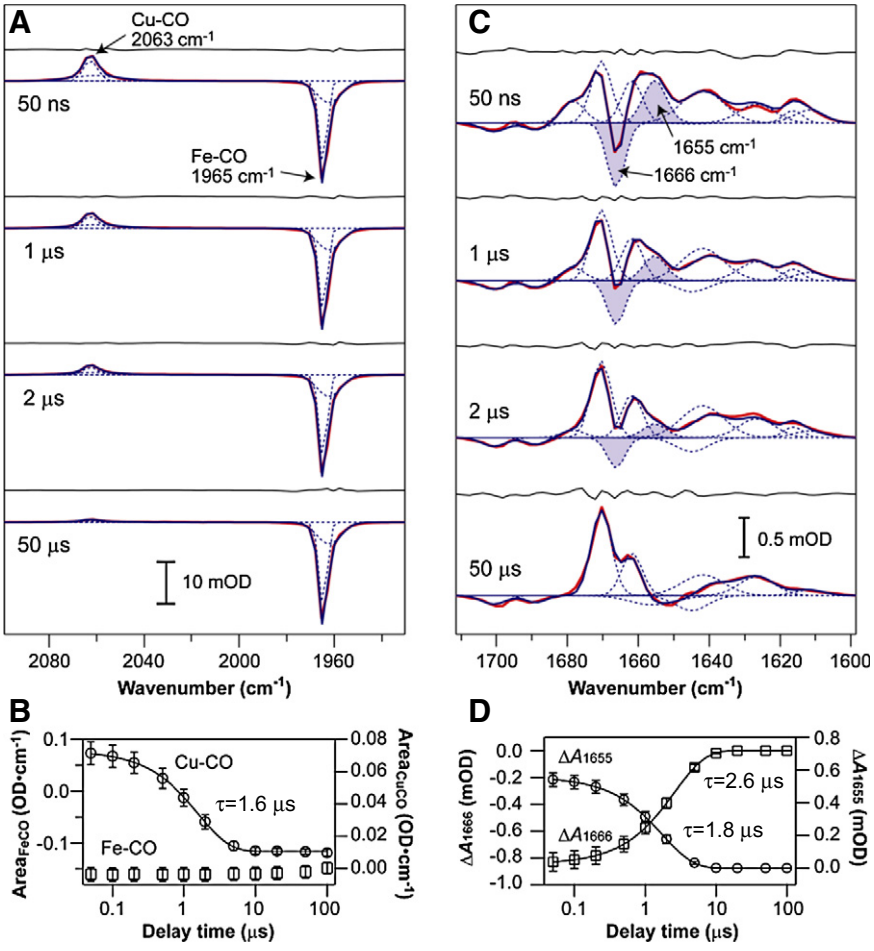

Fig. 5. TRIR difference spectra of CcO in H_2O. Red: measured spectra, blue: Fitted spectra, with each Gaussian component shown as a dotted curve. The fitting residuals are also shown for each spectrum. The protein concentration and optical path-length were 0.72 mM and 100 μm for (A) and 0.68 mM and 13 μm for (C), respectively. The error bars represent the standard deviation (S.D.) of three (B) and five (D) independent experiments performed on different days using differently prepared batches of CcO.
(Reproduced from Ref. [18].)

a lower frequency shift of amide-I. Thus, the 1666(−)/1655(+) cm^{-1} transition strongly suggests that the bulge structure was eliminated and a new hydrogen-bonded C═O was generated. The X-ray structures of bovine CcO showed that the structural change related to the bulge conformation upon CO binding is present only in the segment from Val380 to Ser382 (separated by three C═O groups) in helix X [4]. This strongly supports the assignment of the 1666(−)/1655(+) cm^{-1} band transition to the structural change of Val380 from the bulge to the helix.

Thus, the bulge transfer from Val380 to Ser382 was found to be concomitant with transient CO-binding to Cu_B, and the existence of an 'information-relay system' between the Cu_B site and the gate of the water channel at Ser382 was suggested. This would ensure the H_2O (H^+ source) loading into the hydrogen bond network and timely closing of the water channel. The detailed mechanisms will be discussed in Section 4 in combination with the results obtained from the rR studies.

Additional important information was obtained from carboxyl C═O stretching band, as shown in Fig. 6. The peak/trough bands were observed at 1749/1738 cm^{-1}. Their decay time constants are approximately the same, being 1.1 and 0.7 μs, respectively. To reconstruct the band shapes of all of the observed spectra, at least four bands were necessary, that is, in addition to 1749/1738 cm^{-1}, another two bands were present at close frequencies, 1750/1745 cm^{-1}. The rise time was almost the same (~16 μs) for two pairs. Although there has been a great deal of debate about the number of bands existing in this region [56], the finding confirmed that at least four bands exist in this region. It became clear from the assignment of these bands of bovine heart CcO that the behavior of Glu242 is synchronized with that of helix X, and that the behavior of Asp51 (the exit of the H^+ pump) is slower. Regardless of the fact that this information does not give us further insight into the reaction mechanism, such precise experiments and analysis are potentially able to clarify the detailed behaviors of the residues, even in the region where the bands are complexly overlapped.

3. Resonance Raman spectroscopic studies

In rR spectroscopic studies [78], the excitation wavelength is tuned to the absorption maxima of chromophores in order to potently enhance the Raman intensity. By tuning the excitation wavelength, the vibrational spectra of a proper chromophore can be enhanced, which enables a consideration of even a single bond of the chromophore in a huge protein molecule. In addition, the strong enhancement of Raman intensity allows the study of very dilute solutions of the enzyme and thus examination of short-lived reaction intermediates in small amount.

In the CcO case, the resonance with the Soret- and Q-bands and the CT band [79,80] provides information on the structure around the hemes and the binding state of O_2 toward heme. Furthermore, the electronic structures of the intermediates during the O_2 reduction reaction have been studied extensively and some of the characteristics of each of the intermediate states clarified [2,81–91]. Therefore, the coupling mechanisms between the O_2 reduction and the H^+ pumping have become a main subject of interest. The peripheral groups of hemes make hydrogen bonds with amino acid residues that are related to the H^+ pumping. For example, the formyl group of heme *a* interacts with Arg38, and the farnesylethyl group of heme *a* interacts with Ser382, with both residues located in the H-pathway [1]. Therefore, it became evident that it was necessary to observe the interaction between these heme peripheral groups and the interacting residues during the O_2 reduction.

Since aromatic residues display absorption in a UV region, UV excitation of Raman scattering is expected to be useful to explore protein structural changes involving aromatic residues such as Tyr244 [92] which is covalently bound to His240 at the *ortho* position of the phenoxy ring, and is believed to function in acid/base catalysis for

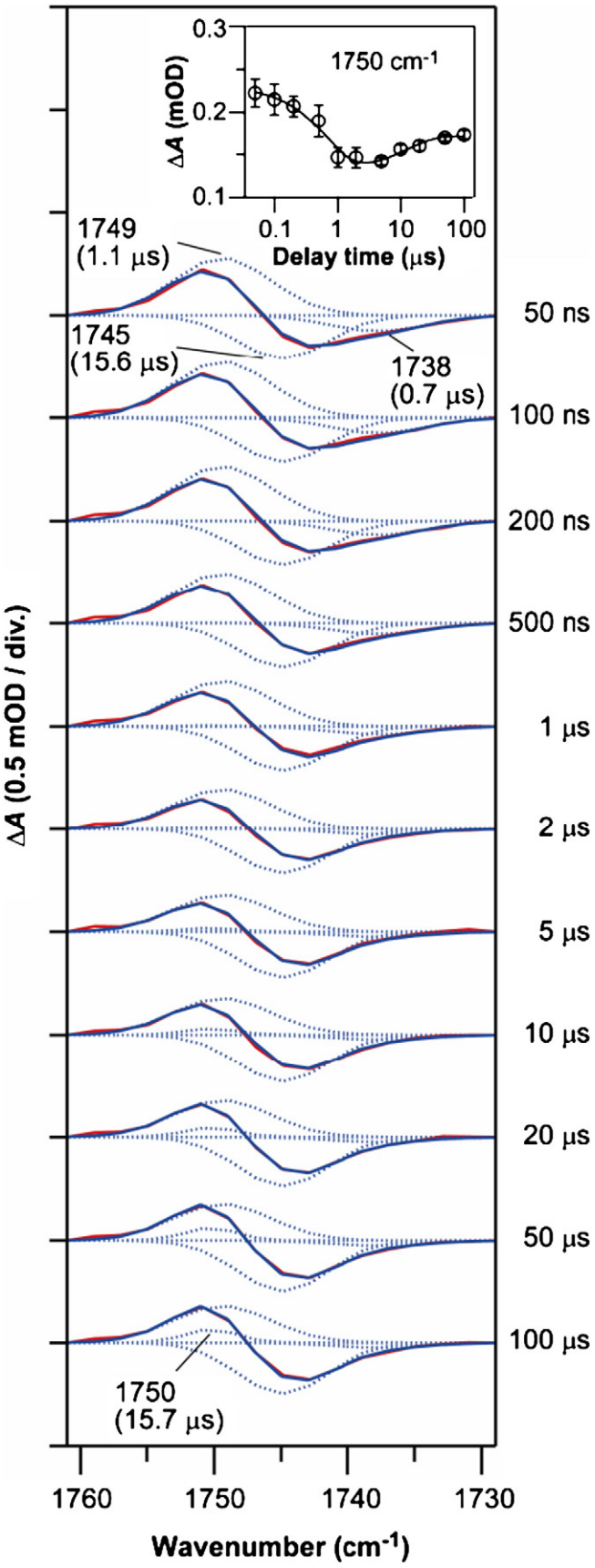

Fig. 6. TRIR difference spectra of CcO in H_2O. in the COOH CO stretching region. Red: measured spectra, blue: Fitted spectra, with each Gaussian component shown as dotted curve. The protein concentration and optical path-length were 0.78 mM and 50 μm. The inset shows a time trace of ΔA at 1750 cm^{-1}. Error bars represent the S.D. of three independent experiments.

dioxygen reduction [93]. Although these aromatic residues can also be observed by IR spectroscopy, the site-specific enhancement of Raman spectroscopy can make the analysis relatively simple, even for such a huge protein.

On the other hand, it is quite important to examine whether the CcO in mitochondria reacts in a way similar to that of the isolated one. To solve this problem, the Raman measurements on intact mitochondria or the CcO contained in phospholipid vesicles (COV) [94–96] were recently undertaken. It is essential in the case of CcO to examine the effects of any electronic field and/or H^+-concentration gradient across the membrane on the protein structure, because the reactivity of CcO is regulated by such factors. For this purpose, rR spectroscopy provides much detailed information on the chromophore. In this section, recent results from rR spectroscopy are briefly reviewed, and then the initial reaction mechanisms of CcO that were elucidated from the combined results of the time-resolved IR and Raman experiments will be summarized.

3.1. Time-resolved resonance Raman (TR^3) studies

There are two types of methods in TR^3 spectroscopy. One is to use two continuous wave (CW) lasers separated by a certain distance for a flowing sample, and the other is to use two pulsed lasers that are fired with a certain time delay.

In the former case, CcO sample must be passed through a cell at a certain speed, and the spectrum is measured by the laser on the down-stream side after the reaction is initiated by the other laser on the up-stream side. The distance between the two lasers and the flow speed determine the time delay after the start of the reaction. The rR scattering is so weak that an extended period of time for accumulation is required in order to obtain high quality rR spectra of the intermediates. However, in the mixed-flow experiments, the time available for accumulation is limited by the amount of the enzyme in the reservoir and is generally insufficient. In the case of CcO, an ingenious method was developed by Ogura [82–86]. This method was designed to specially enable the accumulation of the spectra of the reaction intermediates of O_2 over an extended period of time with a limited amount of enzyme. By using this apparatus, each intermediate was specified by the oxygen-isotope sensitive Raman bands as shown in Fig. 1., with the oxy-species denoted as A ($\nu(Fe-O_2^-) = 571\ cm^{-1}$), peroxy-species denoted as P ($\nu(Fe{=}O^{2-}) = 804\ cm^{-1}$), ferryl-species denoted as F ($\nu(Fe{=}O^{2-}) = 785\ cm^{-1}$) and hydroxyl-species denoted as O ($\nu(Fe-OH) = 450\ cm^{-1}$). When the O_2 reduction is subjected to the MV state ($a^{3+}a_3^{2+}$), the reaction stops at the P intermediate [97]. Such techniques have been proven to be indispensable for the rR spectra of short-lived reaction intermediates with a small population.

The other type of time-resolved measurement is a pump/probe method using two pulsed lasers. This method can be applied to cyclic reactions of a sample containing a spinning cell and is initiated by photolysis due to a pumped pulse. The pulse energy must be low enough not to destroy the sample, and the repetition of the laser determines the upper limit of the time delay. Despite these limitations, this technique has the major advantage of allowing measurements with a quite short time regime (<10 μs) which cannot be achieved by the flow method. The CO photolysis processing of CcO at ambient temperature was pursued with the TR^3 technique using two ns pulse lasers [98,99]. It was reported that the Fe–His stretching (ν_{Fe-His}) mode is located at 221 cm^{-1} between 10 and 100 ns after photodissociation of CO and then exhibits a downshift to 215 cm^{-1}, that which is the frequency of the equilibrium of the fully-reduced form, with a time constant of 0.6 μs. In the case of Mb, this relaxation process takes place on a 100 ps time scale [101], which indicates that tertiary structural changes of a monomeric protein occurred in a 100 ps time regime. This strongly indicates that the Fe–His bond relaxation in CcO is not regulated only by the movement of the His-containing helix, but also by cooperative movements of other parts of the protein, presumably those of the H^+ pumping pathway.

3.2. Heme peripheral groups and their interactions with the surrounding amino acid residues

The peripheral groups of both hemes interact with surrounding amino acid residues that are related to H^+ pumping. Hence, effort has been given to establish the structural markers for the peripheral groups [99,102,103]. Monitoring the marker bands for the propionate groups, which undergo conformational change during the catalytic cycle of CcO, is especially important.

The TR^3 results from CO-photodissociation of CcO [99] showed that the vinyl stretching band (1629 cm^{-1}) of the heme a_3 shifts by 2 cm^{-1} and the vinyl bending mode of heme *a* appears at 435 cm^{-1} instantaneously upon photolysis. Both of the vinyl groups of heme a_3 and heme *a* are located near the bulge structure of helix X. The time profile provides strong evidence for the fact that the conformational change of heme *a* is tightly coupled with the conformational change in the vinyl group of heme a_3. Thus, the frequency shift of the heme *a* vinyl band is deduced to occur through the structural change of heme a_3 upon the release of CO via the interaction between helix X and the vinyl group of heme *a*. These results suggest that both hemes cooperatively control O_2 binding by forming an intermediate conformation for effective H^+ pumping.

Not only the local interactions, but also the effects from the surrounding environment such as those that occur on the membrane, are considered to influence H^+ pump activity. Therefore, the improved rR method has been applied to intact mitochondria and the O_2 activation reaction by CcO has been successfully detected [94,95]. The coordination geometries of the three intermediates (A, P, and F) are essentially the same as the respective species observed for solubilized CcO. However, the lifetime of the oxygenated intermediate in mitochondria was significantly longer than the lifetime of this intermediate determined for solubilized CcO. This phenomenon is due either to the pH effect of the mitochondrial matrix, the effect of ΔpH and/or ΔΨ across the membrane, or the effect of interactions with other membrane components and/or phospholipids. These findings indicate that the surrounding environment may influence the reaction kinetics, but not the local structures.

4. Combined structural results of Raman and IR spectroscopy

The phenomena were observed in the CO photolysis reaction, while what actually occurs physiologically is the reverse process, that is, O_2 binding to heme a_3 followed by H^+ and electron transfer. Although these two processes are not exactly the reverse processes, investigation of the CO photolysis process is expected to give valuable information on the protein response to ligand binding to and dissociation from the BNC [38–55]. The results obtained from the TRIR and TR^3 measurements are summarized first and then are discussed based on the results from the initial stage of O_2 reduction by CcO.

The TRIR experiments (Fig. 5A) showed that CO moves from Fe (heme a_3) to Cu_B just after the photodissociation [18,41–45]. The TR^3 experiments indicated that the heme a_3–His stretching frequency undergoes no change for the initial 100 ns [98,100]. At this stage, the bulge structure of helix X at Ser382 was once more eliminated and a normal α-helix was formed (Fig. 5C, 50 ns). From the MD simulations, when a ligand binds to Cu_B and helix X adopts the normal α-helix, the gate of the water channel is in the "open" state [18]. Therefore, in the reverse process, a ligand binding to heme a_3 changes the helix X structure from the "open" state (normal α-helix) to the "closed" state (the bulge structure at Ser382).

While CO was released into bulk solution with a time constant of 1.6 μs, almost simultaneously (2.6 μs) another bulge structure at Val380 was generated in helix X (Fig. 5C, 1 μs, 2 μs). This indicated

that the escape of CO into the bulk solution and the conversion of the helix structure from the α-helix to the bulge were synchronized. Here, heme a_3 – His stretching gradually shifts from 221 to 215 cm^{-1} with a time constant of 0.6 μs [98,100]. It is noted that the Cu_B-bound CO did not geminately rebind to heme a_3, despite the fact that heme a_3–CO is much more stable than Cu_B–CO in a stationary state at ambient temperatures. This is also against common sense for typical heme proteins, in which several percent of CO geminately rebind to heme after CO-photolysis. Meanwhile, the Fe – His stretching frequency is known to correlate with the O_2 affinity of heme [104,105]. Considering the results from deoxyHb, the low frequency shift from 221 to 215 cm^{-1} corresponds to a 100-fold lowering of the O_2 affinity. These results suggest that in the reverse process in which a ligand that comes into the BNC site, it first binds to Cu_B temporarily and then to heme a_3 according to its affinity. This binding to Cu_B is also thought to cause the structural change in helix X.

On the other hand, the carboxyl group of Glu242 that locates between heme *a* and heme a_3 called the H^+ shuttle, changed in a way that almost synchronized with the structural changes mentioned above, and the carboxyl group of Asp51 located at the exit of the H-pathway responded later (15 μs). The time-dependent difference spectral changes in the COOH region are shown in Fig. 6, where the weaker 1750 cm^{-1} band beside the stronger 1749 cm^{-1} band is evident. The inset shows the time constant of the intensity change to be 15.7 μs. The gating of the H^+ pathway, presumably at Asp51, which must be done in such a way as to maintain $H^+/e^- = 1$ in terms of individual electron transfer, is carried out by heme *a* during the O_2 reduction reactions for four times [4]. Since the processes take place after the O_2 binding to heme a_3, they are different from the present subject of gating, but further studies on the short-lived intermediates of the reaction are required to elucidate the roles of these residues during the reaction.

From the present TRIR and TR^3 observations, the scheme illustrated in Fig. 7 is postulated for the initial process of O_2 binding to heme a_3. In the first place, O_2 binds to Cu_B, but it does not bind to heme a_3, because the O_2 affinity is low at this step (Fig. 7A). At this stage, the bulge structure of helix X is eliminated, where the gate for a water channel is the "open" state, and H_2O is able to enter and exit via this gate. Here, we assume that hydrogen bonding to Ser382 functions as a sensor of the water channel. When Ser382 forms a hydrogen bond with the water channel and changes protein structure, it induces a change in the O_2 affinity of heme a_3 through the helix X and Fe – His bond (Fig. 7B). When a sufficient amount of H_2O (the H^+ source) is supplied to the water channel, the O_2 affinity becomes the highest and O_2 moves from Cu_B to heme a_3 (Fig. 7C). Synchronized with this O_2 binding, the gate of the water channel becomes "closed" and then the O_2 reduction reaction proceeds while the gate retains the closed bulge structure (Fig. 7D). Compared with the O_2 binding kinetics (>10 μs) and the further reactions, the closure of the gate observed here is substantially faster (~1 μs). Thus this process ensures the timely closure of the gate before the reaction starts.

This model shows why the gate is present on the side of the water channel in helix X. From X-ray structural analysis [9], the gate is closed while any kind of ligand is bound to heme a_3. This means that the water channel is closed during the H^+ pumping processes, so an exchange of H_2O (or H_3O^+) between the inside hydrogen bond network and the bulk water on the negative side is possible only when heme a_3 is in the ligand-free FR state. Four H^+ equivalents must enter the channel in the FR state before O_2 binds to heme a_3. When O_2 binds to heme a_3, the gate is closed to prevent backward flow of H_2O (or H_3O^+), until the reaction at heme a_3 is complete.

The model described above may seem to stand in contrast to the well-known models in which the pumped protons are taken up and released one-at-a-time in four separate steps of the reaction cycle [6]. Practically, however, there is no contradiction because the gating occurs before the four separate steps of the reaction. In other words, the present model explains what is happening at the beginning of the reaction, but does not describe intermediate states during the proton pumping reaction process. As has often been observed in the proton pumping protein [106], the migration of water or proton into the entrance of the gate takes place by a diffusionary process, and it is also

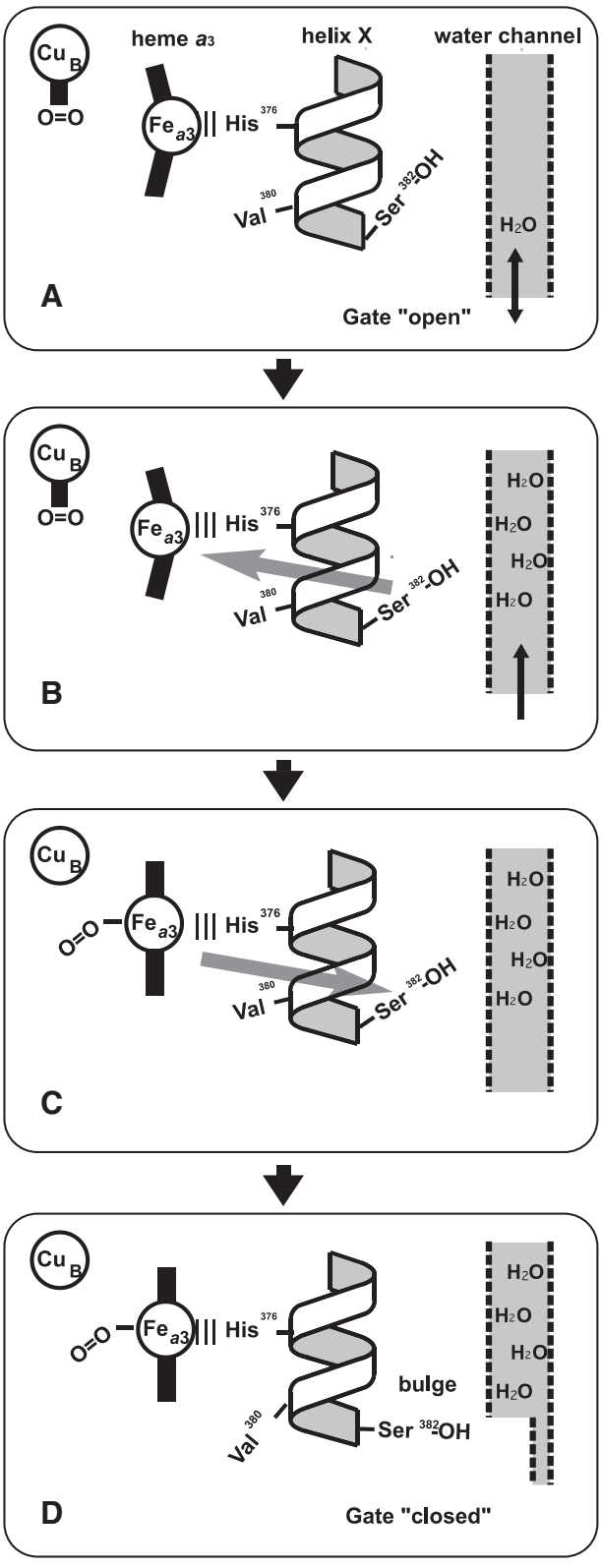

Fig. 7. Proposed mechanism of initial stage of O_2 binding. See the text for details.

the case for CcO [4]. On the other hand since the take-up and release of H^+ are active translocation processes, it is necessary to maintain this diffusion to prevent the back leakage of the H^+ source during the reaction. Thus, gate closure at the initial stage of the reaction and the H^+ take-up and release at each step during the reaction are independent phenomena in the present model. This is distinct from Kubo's model that was reported recently [18], in which both steps are combined in a single process.

The reality of hydrogen bond networks on the upper side of the gate during the reaction is still unknown, since the hydrogen atom is hard to detect by X-ray structural analysis. In the present model, the source of the four H^+ equivalents must pass the gate before the gate closure, but we were unable to determine whether the transferred substance is H_2O or H^+ (H_3O^+). The X-ray structure indicates insufficient room for four free H_2O molecules in the upper side of the gate. Kubo et al. [18] proposed that the substance was H^+ without providing sound structural evidence. If four H^+ equivalents were simultaneously in such a narrow area, the electric repulsion would be excessively large and it is therefore unlikely. We sought evidence for neutralization such as protonation of certain residues, in order to propose a means for the entering of four protons during this process, but it was unsuccessful. It was suggested that the internal water may be replaced during the reaction [35]. When the water molecule is separated into H^+ and OH^- in the pumping reaction, the generated OH^- ions need not be stored there and may escape from the cavity via dynamic movement of the protein side chains.

Although neither the present model nor Kubo's model [18] presents sufficient evidence, H_2O is the more probable substrate at this moment. As the role of the hydrogen bond network is crucially important for the elucidation of the proton pumping mechanisms, it is necessary to perform the experiments that will allow resolution of such questions. Since H_2O molecules inside the protein may be observed independently of bulk water [35,36] and protonation/deprotonation of a specified residue is easily distinguished, TRIR measurements during oxygen reduction reactions are required.

Thus far, the chemical functions of the copper site of CcO have been left to be clarified in the future except for the redox property of Cu_B as a single-electron accepting site. From the new experimental data described here, it became clear that Cu_B not only is a simple e^- donor to the Fe-bound O_2, but also plays a key role in the timely control of the gate of the water channel and also in altering the O_2 affinity at the heme a_3 site.

These results suggest that the hydrogen bonding of Ser382 to the water channel triggers an 'information-relay system' including Cu_B, ligand, heme a_3 and two α-helix turns extending to Ser382. This facilitates the effective collection of H_2O molecules and timely closure of the water channel by the formation of the Ser382 bulge formation. It should be emphasized that the unique roles of Cu_B and the bulge structure of helix X in the H_2O molecule collection and the timely control of the gate of the water channel for the effective energy transduction would have been impossible to discover without using the newly developed TRIR system, which was designed for the investigation of proteins in H_2O under physiological conditions.

5. Future aspects

Recent developments in time-resolved vibrational spectroscopy as well as the other cutting-edge techniques explained here are expected to gain a much more comprehensive picture of the coupling mechanisms underlying CcO function in the future. In particular, TRIR measurements of the reaction in aqueous solution in real-time [19] will provide critical information on the role of the residues and proteins in the H^+ pumping process. Furthermore, additional development in protein manipulation methods, such as in a flow system like the TR^3 system, is also going to be essential for examining the short-lived reaction intermediates.

Acknowledgement

The authors express their gratitude to Dr. Miroru Kubo of RIKEN for the permission of the use of the results shown in Fig. 6 before publication of the original collaborated work.

References

[1] S. Yoshikawa, K. Muramoto, K. Shinzawa-Itoh, Proton-pumping mechanism of cytochrome *c* oxidase, Annu. Rev. Biophys. 40 (2011) 205–223.
[2] T. Kitagawa, T. Ogura, Oxygen activation mechanism at the binuclear site of heme–copper oxidase superfamily as revealed by time-resolved resonance Raman spectroscopy, Prog. Inorg. Chem. 45 (1997) 431–479.
[3] S. Yoshikawa, K. Muramoto, K. Shinzawa-Itoh, H. Aoyama, T. Tsukihara, T. Ogura, K. Shimokata, Y. Katayama, H. Shimada, Reaction mechanism of bovine cytochrome *c* oxidase, Biochim. Biophys. Acta 1757 (2006) 395–400.
[4] T. Tsukihara, K. Shimokata, Y. Katayama, H. Shimada, K. Muramoto, H. Aoyama, M. Mochizuki, K. Shinzawa-Itoh, E. Yamashita, M. Yao, Y. Ishimura, S. Yoshikawa, The low-spin heme of cytochrome *c* oxidase as the driving element of the proton-pumping process, Proc. Natl. Acad. Sci. U. S. A. 100 (2003) 15304–15309.
[5] K. Shimokata, Y. Katayama, H. Murayama, M. Suematsu, T. Tsukihara, K. Muramoto, H. Aoyama, S. Yoshikawa, H. Shimada, The proton pumping pathway of bovine heart cytochrome *c* oxidase, Proc. Natl. Acad. Sci. U. S. A. 104 (2007) 4200–4205.
[6] S. Papa, M. Lorusso, M. di Paola, Cooperativity and flexibility of the protonmotive activity of mitochondrial respiratory chain, Biochim. Biophys. Acta 1757 (2006) 428–436.
[7] T. Tsukihara, H. Aoyama, E. Yamashita, T. Tomizaki, H. Yamaguchi, K. Shinzawa-Itoh, R. Nakashima, R. Yaono, S. Yoshikawa, The whole structure of the 13-subunit oxidized cytochrome *c* oxidase at 2.8 Å, Science 272 (1996) 1136–1144.
[8] S. Yoshikawa, K. Shinzawa-Itoh, R. Nakashima, R. Yaono, E. Yamashita, N. Inoue, M. Yao, M.J. Fei, C.P. Libeu, T. Mizushima, H. Yamaguchi, T. Tomizaki, T. Tsukihara, Redox-coupled crystal structural changes in bovine heart cytochrome *c* oxidase, Science 280 (1998) 1723–1729.
[9] K. Muramoto, K. Ohta, K. Shinzawa-Itoh, K. Kanda, M. Taniguchi, H. Nabekura, E. Yamashita, T. Tsukihara, S. Yoshikawa, Bovine cytochrome *c* oxidase structures enable O_2 reduction with minimization of reactive oxygens and provide a proton-pumping gate, Proc. Natl. Acad. Sci. U. S. A. 107 (2010) 7740–7745.
[10] S. Iwata, C. Ostermeier, B. Ludwig, H. Michel, Structure at 2.8 Å resolution of cytochrome *c* oxidase from *Paracoccus denitrificans*, Nature 376 (1995) 660–669.
[11] M. Svensson-Ek, J. Abramson, G. Larsson, S. Törnroth, P. Brzezinski, S. Iwata, The X-ray crystal structures of wild-type and EQ(I-286) mutant cytochrome *c* oxidases from *Rhodobacter sphaeroides*, J. Mol. Biol. 321 (2002) 329–339.
[12] S. Yoshikawa, K. Muramoto, K. Shinzawa-Itoh, The O_2 reduction and proton pumping gate mechanism of bovine heart cytochrome *c* oxidase, Biochim. Biophys. Acta 1807 (2011) 1279–1286.
[13] G.T. Babcock, How oxygen is activated and reduced in respiration, Proc. Natl. Acad. Sci. U. S. A. 96 (1999) 12971–12973.
[14] G.T. Babcock, M. Wikström, Oxygen activation and the conservation of energy in cell respiration, Nature 356 (1992) 301–309.
[15] P.R. Rich, The molecular machinery of Keilin's respiratory chain, Biochem. Soc. Trans. 31 (2003) 1095–1105.
[16] J.P. Hosler, S. Ferguson-Miller, D.A. Mills, Energy transduction: proton transfer through the respiratory complexes, Annu. Rev. Biochem. 75 (2006) 165–187.
[17] P. Brzezinski, P. Ädelroth, Design principles of proton-pumping haem–copper oxidases, Curr. Opin. Struct. Biol. 16 (2006) 465–472.
[18] M. Kubo, S. Nakashima, S. Yamaguchi, T. Ogura, M. Mochizuki, J. Kang, M. Tateno, K. Shinzawa-Itoh, K. Kato, S. Yoshikawa, J. Biol. Chem. 288 (2013) 30259–30269.
[19] S. Nakashima, M. Kubo, K. Shinzawa-Itoh, S. Yoshikawa, T. Ogura, High-sensitivity Nanosecond Time-resolved IR Spectrometer for Studying Protein Dynamics in Aqueous Solution, 2014. (submitted for publication).
[20] P. Hellwig, B. Rost, U. Kaiser, C. Ostermeier, H. Michel, W. Mäntele, Carboxyl group protonation upon reduction of the *Paracoccus denitrificans* cytochrome *c* oxidase: direct evidence by FTIR spectroscopy, FEBS Lett. 385 (1996) 53–57.
[21] P. Hellwig, J. Behr, C. Ostermeier, O.M.H. Richter, U. Pfitzner, A. Odenwald, B. Ludwig, H. Michel, W. Mäntele, Involvement of glutamic acid 278 in the redox reaction of the cytochrome *c* oxidase from *Paracoccus denitrificans* investigated by FTIR spectroscopy, Biochemistry 37 (1998) 7390–7399.
[22] H. Marrero, K.J. Rothschild, Bacteriorhodopsin's M_{412} and BR_{605} protein conformations are similar, FEBS Lett. 223 (1987) 289–293.
[23] P.R. Rich, A. Maréchal, Carboxyl group functions in the heme–copper oxidases: information from mid-IR vibrational spectroscopy, Biochim. Biophys. Acta 1777 (2008) 912–918.
[24] J. Behr, P. Hellwig, W. Mäntele, H. Michel, Redox dependent changes at the heme propionates in cytochrome *c* oxidase from *Paracoccus denitrificans*: direct evidence from FTIR difference spectroscopy in combination with heme propionate ^{13}C labeling, Biochemistry 37 (1998) 7400–7406.
[25] S.Y. Venyaminov, N.N. Kalnin, Quantitative IR spectrophotometry of peptide compounds in water (H_2O) solutions. I. Spectral parameters of amino acid residue absorption bands, Biopolymers 30 (1990) 1243–1257.
[26] A. Barth, The infrared absorption of amino acid side chains, Prog. Biophys. Mol. Biol. 74 (2000) 141–173.
[27] A. Barth, Infrared spectroscopy of proteins, Biochim. Biophys. Acta 1767 (2007) 1073–1101.
[28] P.R. Rich, M. Iwaki, Infrared protein spectroscopy as a tool to study protonation reactions within proteins, in: M. Wikström (Ed.), Biophysical and Structural Aspects

of Bioenergetics, The Royal Society of Chemistry, Cambridge, U.K., 2005, pp. 314–333.
[29] H. Torii, M. Tasumi, Model calculations on the amide-I infrared bands of globular proteins, J. Chem. Phys. 96 (1992) 3379–3387.
[30] H. Torii, M. Tasumi, Application of the three-dimensional doorway-state theory to analyses of the amide-I infrared bands of globular proteins, J. Chem. Phys. 97 (1992) 92–98.
[31] P. Hellwig, U. Pfitzner, J. Behr, B. Rost, R.P. Pesavento, W.V. Donk, R.B. Gennis, H. Michel, B. Ludwig, W. Mäntele, Vibrational modes of tyrosines in cytochrome *c* oxidase from *Paracoccus denitrificans*: FTIR and electrochemical studies on Tyr-D_4-labeled and on Tyr280His and Tyr35Phe mutant enzymes, Biochemistry 41 (2002) 9116–9125.
[32] M.M. Pereira, F.L. Sousa, M. Teixeira, R.M. Nyquist, J. Heberle, A tyrosine residue deprotonates during oxygen reduction by the caa_3 reductase from *Rhodothermus marinus*, FEBS Lett. 580 (2006) 1350–1354.
[33] M. Iwaki, A. Puustinen, M. Wikström, P.R. Rich, Structural and chemical changes of the P_M intermediate of *Paracoccus denitrificans* cytochrome *c* oxidase revealed by IR spectroscopy with labelled tyrosines and histidine, Biochemistry 45 (2006) 10873–10885.
[34] H. Kandori, Role of internal water molecules in bacteriorhodopsin, Biochim. Biophys. Acta 1460 (2000) 177–191.
[35] F. Garczarek, K. Gerwert, Functional waters in intraprotein proton transfer monitored by FTIR difference spectroscopy, Nature 439 (2006) 109–112.
[36] A. Maréchal, P.R. Rich, Water molecule reorganization in cytochrome *c* oxidase revealed by FTIR spectroscopy, Proc. Natl. Acad. Sci. U. S. A. 108 (2011) 8634–8638.
[37] P.R. Rich, M. Iwaki, Methods to probe protein transitions with ATR infrared spectroscopy, Mol. Biosyst. 3 (2007) 398–407.
[38] J.M. Chalmers, P.R. Griffiths (Eds.), Handbook of Vibrational Spectroscopy, vol. 1, John Willey & Sons, Ltd., 2002
[39] S. Yoshikawa, M.G. Choc, M.C. O'Toole, W.S. Caughey, An infrared study of CO binding to heart cytochrome *c* oxidase and hemoglobin A. Implications re O_2 reactions, J. Biol. Chem. 252 (1977) 5498–5508.
[40] J.O. Alben, P.P. Moh, F.G. Fiamingo, R.A. Altschuld, Cytochrome oxidase a_3 heme and copper observed by low-temperature Fourier transform infrared spectroscopy of the CO complex, Proc. Natl. Acad. Sci. U. S. A. 78 (1981) 234–237.
[41] R.B. Dyer, O. Einarsdóttir, P.M. Killough, J.J. López-Garriga, W.H. Woodruff, Transient binding of photodissociated CO to Cu_B^+ of eukaryotic cytochrome oxidase at ambient temperature. Direct evidence from time-resolved infrared spectroscopy, J. Am. Chem. Soc. 111 (1989) 7657–7659.
[42] O. Einarsdóttir, P.M. Killough, J.A. Fee, W.H. Woodruff, An infrared study of the binding and photodissociation of carbon monoxide in cytochrome ba_3 from *Thermus thermophilus*, J. Biol. Chem. 264 (1989) 2405–2408.
[43] R.B. Dyer, K.A. Peterson, P.O. Stoutland, W.H. Woodruff, Ultrafast photoinduced ligand transfer in carbonmonoxy cytochrome *c* oxidase. Observation by picosecond infrared spectroscopy, J. Am. Chem. Soc. 113 (1991) 6276–6277.
[44] O. Einarsdóttir, R.B. Dyer, D.D. Lemon, P.M. Killough, S.M. Hubig, S.J. Atherton, J.J. Lbpez-Garriga, G. Palmer, W.H. Woodruff, Photodissociation and recombination of carbonmonoxy cytochrome oxidase: dynamics from picoseconds to kiloseconds, Biochemistry 32 (1993) 12013–12024.
[45] R.B. Dyer, K.A. Peterson, P.O. Stoutland, W.H. Woodruff, Picosecond infrared study of the photodynamics of carbonmonoxy-cytochrome *c* oxidase, Biochemistry 33 (1994) 500–507.
[46] D.M. Mitchell, J.P. Shapleigh, A.M. Archer, J.O. Alben, R.B. Gennis, A pH-dependent polarity change at the binuclear center of reduced cytochrome *c* oxidase detected by FTIR difference spectroscopy of the CO adduct, Biochemistry 35 (1996) 9446–9450.
[47] D.M. Mitchell, J.D. Muller, R.B. Gennis, G.U. Nienhaus, FTIR study of conformational substates in the CO adduct of cytochrome *c* oxidase from *Rhodobacter sphaeroides*, Biochemistry 35 (1996) 16782–16788.
[48] E.D. Dodson, X.-J. Zhao, W.S. Caughey, C.M. Elliott, Redox dependent interactions of the metal sites in Carbon monoxide-bound cytochrome *c* oxidase monitored by infrared and UV/visible spectroelectrochemical methods, Biochemistry 35 (1996) 444–452.
[49] A. Puustinen, J.A. Bailey, R.B. Dyer, S.L. Mecklenburg, M. Wikström, W.H. Woodruff, Fourier transform infrared evidence for connectivity between Cu_B and glutamic acid 286 in cytochrome bo_3 from *E. coli*, Biochemistry 36 (1997) 13195–13200.
[50] B. Rost, J. Behr, P. Hellwig, O.-M.H. Richter, B. Ludwig, H. Michel, W. Mäntele, Time-resolved FT-IR studies on the CO adduct of *Paracoccus denitrificans* cytochrome *c* oxidase: comparison of the fully reduced and the mixed valence form, Biochemistry 38 (1999) 7565–7571.
[51] P.R. Rich, J. Breton, S. Jünemann, P. Heathcote, Protonation reactions in relation to the coupling mechanism of bovine cytochrome *c* oxidase, Biochim. Biophys. Acta 1459 (2000) 475–480.
[52] P.R. Rich, J. Breton, FTIR studies of the CO and cyanide compounds of fully reduced bovine cytochrome *c* oxidase, Biochemistry 40 (2001) 6441–6449.
[53] J.A. Bailey, F.L. Tomson, S.L. Mecklenburg, G.M. MacDonald, A. Katsonouri, A. Puustinen, R.B. Gennis, W.H. Woodruff, R.B. Dyer, Time-resolved step-scan Fourier transform infrared spectroscopy of the CO adducts of bovine cytochrome *c* oxidase and cytochrome bo_3 from *Escherichia coli*, Biochemistry 41 (2002) 2675–2683.
[54] D. Heitbrink, H. Sigurdson, C. Bolwien, P. Brzezinski, J. Heberle, Transient binding of CO to Cu_B in cytochrome *c* oxidase is dynamically linked to structural changes around a carboxyl group: a time-resolved step-scan Fourier transform infrared investigation, Biophys. J. 82 (2002) 1–10.
[55] C. Koutsoupakis, T. Soulimane, C. Varotsis, Ligand binding in a docking site of cytochrome *c* oxidase: a time-resolved step-scan Fourier transform infrared study, J. Am. Chem. Soc. 125 (2003) 14728–14732.
[56] D. Okuno, T. Iwase, K. Shinzawa-Itoh, S. Yoshikawa, T. Kitagawa, FTIR detection of protonation/deprotonation of key carboxyl side chains caused by redox change of the Cu_A–heme a moiety and ligand dissociation from the heme a_3–Cu_B center of bovine heart cytochrome *c* oxidase, J. Am. Chem. Soc. 125 (2003) 7209–7218.
[57] B.H. McMahon, M. Fabian, F. Tomson, T.P. Causgrove, J.A. Bailey, F.N. Rein, R.B. Dyer, G. Palmer, R.B. Gennis, W.H. Woodruff, FTIR studies of internal proton transfer reactions linked to inter-heme electron transfer in bovine cytochrome *c* oxidase, Biochim. Biophys. Acta 1655 (2004) 321–331.
[58] C. Koutsoupakis, E. Pinakoulaki, S. Stavrakis, V. Daskalakis, C. Varotsis, Time-resolved step-scan Fourier transform infrared investigation of heme–copper oxidases: implications for O_2 input and H_2O/H^+ output channels, Biochim. Biophys. Acta 1655 (2004) 347–352.
[59] E.A. Gorbikova, M. Wikström, M.I. Verkhovsky, The protonation state of the cross-linked tyrosine during the catalytic cycle of cytochrome *c* oxidase, J. Biol. Chem. 283 (2008) 34907–34912.
[60] E.A. Gorbikova, I. Belevich, M. Wikström, M.I. Verkhovsky, The proton donor for O – O bond scission by cytochrome *c* oxidase, Proc. Natl. Acad. Sci. U. S. A. 105 (2008) 10733–10737.
[61] P. Hellwig, C. Ostermeier, H. Michel, B. Ludwig, W. Mäntele, Electrochemically induced FT-IR difference spectra of the two- and four-subunit cytochrome *c* oxidase from *P. denitrificans* reveal identical conformational changes upon redox transitions, Biochim. Biophys. Acta 1409 (1998) 107–112.
[62] P. Hellwig, T. Soulimane, G. Buse, W. Mäntele, Similarities and dissimilarities in the structure–function relation between the cytochrome *c* oxidase from bovine heart and from *Paracoccus denitrificans* as revealed by FT-IR difference spectroscopy, FEBS Lett. 458 (1999) 83–86.
[63] P. Hellwig, S. Grzybek, J. Behr, B. Ludwig, H. Michel, W. Mäntele, Electrochemical and ultraviolet/visible/infrared spectroscopic analysis of heme a and a_3 redox reactions in the cytochrome *c* oxidase from *Paracoccus denitrificans*: separation of heme *a* and a_3 contributions and assignment of vibrational modes, Biochemistry 38 (1999) 1685–1694.
[64] J. Behr, H. Michel, W. Mäntele, P. Hellwig, Functional properties of the heme propionates in cytochrome *c* oxidase from *Paracoccus denitrificans*. Evidence from FTIR difference spectroscopy and site-directed mutagenesis, Biochemistry 39 (2000) 1356–1363.
[65] P. Hellwig, T. Soulimane, G. Buse, W. Mantele, Electrochemical, FTIR, and UV/VIS Spectroscopic Properties of the ba_3 Oxidase from *Thermus thermophilus*, Biochemistry 38 (1999) 9648–9658.
[66] P. Hellwig, C.M. Gomes, M. Teixeira, FTIR spectroscopic characterization of the cytochrome aa_3 from *Acidianus ambivalens*: evidence for the involvement of acidic residues in redox coupled proton translocation, Biochemistry 42 (2003) 6179–6184.
[67] E.A. Gorbikova, N.P. Belevich, M. Wikström, M.I. Verkhovsky, Protolytic reactions on reduction of cytochrome *c* oxidase studied by ATR-FTIR spectroscopy, Biochemistry 46 (2007) 4177–4183.
[68] E.A. Gorbikova, N.P. Belevich, M. Wikström, M.I. Verkhovsky, Time-resolved ATR-FTIR spectroscopy of the oxygen reaction in the D124N mutant of cytochrome *c* oxidase from *Paracoccus denitrificans*, Biochemistry 46 (2007) 13141–13148.
[69] R.M. Nyquist, D. Heitbrink, C. Bolwien, R.B. Gennis, J. Heberle, Direct observation of protonation reactions during the catalytic cycle of cytochrome *c* oxidase, Proc. Natl. Acad. Sci. U. S. A. 100 (2003) 8715–8720.
[70] M. Iwaki, A. Puustinen, M. Wikström, P.R. Rich, ATR-FTIR spectroscopy of the P_M and F intermediates of bovine and *Paracoccus denitrificans* cytochrome *c* oxidase, Biochemistry 42 (2003) 8809–8817.
[71] M. Iwaki, A. Puustinen, M. Wikström, P.R. Rich, ATR-FTIR spectroscopy and isotope labelling of the P_M intermediate of *Paracoccus denitrificans* cytochrome *c* oxidase, Biochemistry 43 (2004) 14370–14378.
[72] M. Iwaki, P.R. Rich, Direct detection of formate ligation in cytochrome *c* oxidase by ATR-FTIR spectroscopy, J. Am. Chem. Soc. 126 (2004) 2386–2389.
[73] D. Magana, D. Parul, R.B. Dyer, A.P. Shreve, Implementation of time-resolved step-scan Fourier transform infrared (FT-IR) spectroscopy using a kHz repetition rate pump laser, Appl. Spectrosc. 65 (2011) 535–542.
[74] L.J.G.W. van Wilderen, M.A. van der Horst, I.H.M. van Stokkum, K.J. Hellingwerf, R. van Grondelle, Ultrafast infrared spectroscopy reveals a key step for successful entry into the photocycle for photoactive yellow protein, Proc. Natl. Acad. Sci. U. S. A. 103 (2006) 15050–15055.
[75] M.L. Groot, L.J.G.W. van Wilderen, D.S. Larsen, M.A. van der Horst, I.H.M. van Stokkum, K.J. Hellingwerf, R. van Grondelle, Initial steps of signal generation in photoactive yellow protein revealed with femtosecond mid-infrared spectroscopy, Biochemistry 42 (2003) 10054–10059.
[76] M.D. Donato, A.D. Stahl, I.H.M. van Stokkum, R. van Grondelle, M.L. Groot, Cofactors involved in light-driven charge separation in photosystem I identified by subpicosecond infrared spectroscopy, Biochemistry 50 (2011) 480–490.
[77] J. Herbst, K. Heyne, R. Diller, Femtosecond infrared spectroscopy of bacteriorhodopsin chromophore isomerization, Science 297 (2002) 822–825.
[78] K. Nakamoto, Infrared and Raman Spectra of Inorganic and Coordination Compounds, Applications in Coordination, Organometallic, and Bioinorganic Chemistry, sixth ed. John Wiley & Sons, Inc., Hoboken, 2009.
[79] K. Ikemura, M. Mukai, H. Shimada, T. Tsukihara, S. Yamaguchi, K. Shinzawa-Itoh, S. Yoshikawa, T. Ogura, Red-excitation resonance Raman analysis of the $\nu_{Fe=O}$ mode of ferryl-oxo hemoproteins, J. Am. Chem. Soc. 130 (2008) 14384–14385.
[80] M. Sakaguchi, K. Shinzawa-Itoh, S. Yoshikawa, T. Ogura, A resonance Raman band assignable to the O – O stretching mode in the resting oxidized state of bovine heart cytochrome *c* oxidase, J. Bioenerg. Biomembr. 42 (2010) 241–243.
[81] T. Ogura, S. Yoshikawa, T. Kitagawa, Resonance Raman study on photoreduction of cytochrome *c* oxidase distinction of cytochrome *a* and cytochrome a_3 in the intermediate oxidation states, Biochemistry 24 (1985) 7746–7752.

[82] T. Ogura, S. Yoshikawa, T. Kitagawa, Raman/absorption simultaneous measurements for cytochrome oxidase compound A at room temperature with a novel flow apparatus, Biochemistry 28 (1989) 8022–8027.
[83] T. Ogura, S. Takahashi, K. Shinzawa-Itoh, S. Yoshikawa, T. Kitagawa, Observation of the $Fe^{II}-O_2$ stretching Raman band for cytochrome oxidase compound A at ambient temperature, J. Am. Chem. Soc. 112 (1990) 5630–5631.
[84] T. Ogura, S. Takahashi, S. Hirota, K. Shinzawa-Itoh, S. Yoshikawa, E.H. Appelman, T. Kitagawa, Time-resolved resonance Raman elucidation of the pathway for dioxygen reduction by cytochrome *c* oxidase, J. Am. Chem. Soc. 115 (1993) 8527–8536.
[85] T. Ogura, S. Hirota, D.A. Proshlyakov, K. Shinzawa-Itoh, S. Yoshikawa, T. Kitagawa, Time-resolved resonance Raman evidence for tight coupling between electron transfer and proton pumping of cytochrome *c* oxidase upon the change from the Fe^{V} oxidation level to the Fe^{IV} oxidation level, J. Am. Chem. Soc. 118 (1996) 5443–5449.
[86] S.W. Han, Y.C. Ching, D.L. Rousseau, Primary intermediate in the reaction of oxygen with fully reduced cytochrome *c* oxidase, Proc. Natl. Acad. Sci. U. S. A. 87 (1990) 2491–2495.
[87] S.H. Han, Y.C. Ching, D.L. Rousseau, Cytochrome c oxidase: decay of the primary oxygen intermediate involves direct electron transfer from cytochrome a, Proc. Natl. Acad. Sci. U. S. A. 87 (1990) 8408–8412.
[88] S. Han, Y.C. Ching, D.L. Rousseau, Ferryl and hydroxy intermediates in the reaction of oxygen with reduced cytochrome *c* oxidase, Nature 348 (1990) 89–90.
[89] G.T. Babcock, J.M. Jean, L.N. Johnston, G. Palmer, W.H. Woodruff, Time-resolved resonance Raman spectroscopy of transient species formed during the oxidation of cytochrome oxidase by dioxygen, J. Am. Chem. Soc. 106 (1984) 8305–8306.
[90] C. Varotsis, W.H. Woodruff, G.T. Babcock, Time-resolved Raman detection of ν(Fe–O) in an early intermediate in the reduction of oxygen by cytochrome oxidase, J. Am. Chem. Soc. 111 (1989) 6439–6440.
[91] C.A. Varotsist, G.T. Babcock, Photolytic activity of early intermediates in dioxygen activation and reduction by cytochrome oxidase, J. Am. Chem. Soc. 117 (1995) 11260–11269.
[92] M. Aki, T. Ogura, K. Shinzawa-Itoh, S. Yoshikawa, T. Kitagawa, A new measurement system for UV resonance Raman spectra of large proteins and its application to cytochrome *c* oxidase, J. Phys. Chem. B 104 (2000) 10765–10774.
[93] M.A. Yu, T. Egawa, K. Shinzawa-Itoh, S. Yoshikawa, V. Guallar, S.R. Yeh, D.L. Rousseau, G.J. Gerfen, Two tyrosyl radicals stabilize high oxidation states in cytochrome *c* oxidase for efficient energy conservation and proton translocation, J. Am. Chem. Soc. 134 (2012) 4753–4761.
[94] T. Takahashi, S. Kuroiwa, T. Ogura, S. Yoshikawa, Probing the oxygen activation reaction in intact whole mitochondria through analysis of molecular vibrations, J. Am. Chem. Soc. 127 (2005) 9970–9971.
[95] T. Ogura, Resonance Raman applications in investigations of cytochrome *c* oxidase, Biochim. Biophys. Acta 1817 (2012) 575–578.
[96] T. Nomura, S. Yanagisawa, K. Shinzawa-Itoh, S. Yoshikawa, T. Ogura, Effects of Proton Motive Force on the Structure and Dynamics of Cytochrome *c* Oxidase, 2014. (submitted for publication).
[97] K. Oda, T. Ogura, E.H. Appelman, S. Yoshikawa, The intrinsic stability of the second intermediate following the dioxygen-bound form in the O_2 reduction by cytochrome *c* oxidase, FEBS Lett. 570 (2004) 161–165.
[98] E.W. Findsen, J. Centeno, G.T. Babcock, M.R. Ondrias, Cytochrome a_3 hemepocket relaxation subsequent to ligand photolysis from cytochrome oxidase, J. Am. Chem. Soc. 109 (1987) 5367–5372.
[99] I. Ishigami, T. Nishigaki, K. Shinzawa-Itoh, S. Yoshikawa, S. Nakashima, T. Ogura, An intermediate conformational state during ligand binding to cytochrome *c* oxidase detected by time-resolved resonance Raman analyses of hone peripheral groups, Chem. Lett. 41 (2012) 178–180.
[100] S. Nakashima, I. Ishigami, K. Shinzawa-Itoh, S. Yoshikawa, T. Ogura, Time-resolved Resonance Raman Study on the Relaxation Process Subsequent to CO Photolysis from Cytochrome *c* Oxidase, 2014. (submitted for publication).
[101] Y. Mizutani, T. Kitagawa, Ultrafast structural relaxation of myoglobin following photodissociation of carbon monoxide probed by time-resolved resonance Raman spectroscopy, J. Phys. Chem. B 105 (2001) 10992–10999.
[102] T. Egawa, H.J. Lee, H. Ji, R.B. Gennis, S.R. Yeh, D.L. Rousseau, Identification of heme propionate vibrational modes in the resonance Raman spectra of cytochrome *c* oxidase, Anal. Biochem. 394 (2009) 141–143.
[103] T. Egawa, S. Yeh, D.L. Rousseau, Redox-controlled proton gating in bovine cytochrome *c* oxidase, PLoS ONE 8 (2013) 1–10.
[104] K. Nagai, T. Kitagawa, H. Morimoto, Quaternary structures and low frequency molecular vibrations of haems of deoxy and oxyhaemoglobin studied by resonance Raman scattering, J. Mol. Biol. 136 (1980) 271–289.
[105] S. Matsukawa, K. Mawatari, Y. Yoneyama, T. Kitagawa, Correlation between the iron–histidine stretching frequencies and oxygen affinity of hemoglobins. A continuous strain model, J. Am. Chem. Soc. 107 (1985) 1108–1113.
[106] O.P. Ernst, D.T. Lodowski, M. Elstner, P. Hegemann, L.S. Brown, H. Kandori, Microbial and animal rhodopsins: structures, functions, and molecular mechanisms, Chem. Rev. 114 (2014) 126–163.